

## **Bone Mineral Density Measurement for Detection of Bone Cancer Using Recurrent**

Meenakshi Shunmugam<sup>a</sup>, Chanda Venkata Alluri Hema Sudheer<sup>b</sup>, Doddaka Sri Vishnu Yadav<sup>c</sup>, Jampana Yeswanth Prudhvi Raju<sup>d</sup>

<sup>a</sup> Assistant Professor, Department of Electronics and Communication Engineering, R.M.K. Engineering College, Kavaraipettai, Tamilnadu, India.

<sup>b,c,d</sup> Student, Department of Electronics and Communication Engineering, R.M.K. Engineering College, Kavaraipettai, Tamilnadu, India

### **Abstract**

Recently, the number of people affected by bone cancer is increasing at a rapid rate. This type of cancer can be cured easily, if identified at earlier stages. Modern imaging techniques are popularly used for the diagnosis of bone cancer. In this research, we propose a new methodology for the identification of bone cancer. In this methodology, the first step is the acquisition of bone images using imaging techniques. The next step is the filtration using 2D Hybrid Bilateral filter. The third step is enhancement using proposed Edge Preservation based Contrast and Brightness Equalization (EPCBE) algorithm. This algorithm was designed such that histogram equalization was done with the aim to preserve the edge information of the images. The next step is the clustering which is performed using Improved Fuzzy C Expectation Maximization (IFCEM) algorithm and thresholding is done using adaptive Otsu (AO) thresholding algorithm. Then, the Grey level Co-occurrence matrix (GLCM) and Grey level difference method (GLDM) matrices are extracted. From these matrices, various statistical features are extracted. Finally, the classification is done using RNN network architecture. The proposed methodology achieved robust results in terms of various evaluation metrics like mean square error, Jaccard coefficient, specificity, recall etc. In particular, the proposed scheme achieved minimal mean square error of 0.87, high Jaccard coefficient of 0.761, high specificity of 96.25% and highest recall rate of 96.52%.

**Keywords:** Bilateral filter, Otsu thresholding, bone cancer, Jaccard coefficient, GLCM

### **1. Introduction**

Cancer is a deadly disease that has high death rate. It is estimated that by the year 2030, the number of cases having cancer will be around 25 million [1]. Bone cancer accounts to about 0.2% of cancer diseases in the world. The people with this ailment suffer from severe pain. The survival rate of this type of cancer is high when the diagnosis is done at an early stage. The survival rate of bone cancer with early diagnosis is around 62.3% [2].

Long term survival of these patients is possible using treatments based on chemoradiotherapy. Recently, treatments based on nano technology is found to produce better survival rates. Here, the carriers for the treatment are in the form of nano particles [3]. Over the past few years, the diagnosis of bone cancer is successful with an increased rate of around 53% using imaging techniques. Various imaging devices like CT scan, MRI scan, etc., are performed to capture the images of bone cancer [4].

The images captured using these devices are processed to obtain suitable inferences. These images contain more noise components and hence cannot be used directly. These noise components are removed using suitable filtration techniques. Filtration is done using image processing filters [5]. These filtered images are then enhanced to produce suitable contrast images. To identify the region of interest, segmentation techniques are opted. Segmentation is done based on clustering and thresholding [6].

From the segmented results, classification is done to identify the malignant cases. Long term treatment of malignant bone cancer cases leads to skeletal complications in the patients. To reduce such complications, bisphosphonates are used [7]. These are some molecular components that are injected to the surface of the bone to reduce the risks involved in the long-term treatment of the bone cancer. A technique called bone scintigraphy is used recently for the identification of bone cancer [8].

The bone scintigraphy imaging technique is highly sensitive. Further, the cost of this technique is low with low value of accuracy rate. This is due to the fact that, this technique is not capable of distinguishing between the tumor and infections [9]. Variety of nanostructures are employed for the identification of bone cancer. These structures are also used for the delivery of drugs to the target bone regions. Further, they are used for the regeneration of the bone cells. The accuracy of using the nano structures is very high [10].

Hence, in this research we propose a novel framework for detection of bone cancer using imaging techniques.

The overall contributions of this paper are fourfold:

- a) A new classification framework for the classification of bone cancer images is presented.
- b) A novel image filtration technique using Hybrid Bilateral filter is performed.
- c) A new image clustering technique using Improved Fuzzy C Expectation Maximization (IFCEM) algorithm is presented.
- d) The proposed framework was evaluated quantitatively using metrics like MSE, PSNR, Jaccard coefficient, Dice coefficient, accuracy, specificity, precision, recall, precision and classification time.

## 2. Related works

Bandyopadhyay et al. [11] has proposed a scheme for the assessment of bone cancer using pattern analysis technique. The long bone X-ray images were employed as input for the analysis. The difference in the bone texture of the affected and non-affected regions were used for the identification of bone cancer. Urbano et al. [12] has presented a system in which breast cancer lesions were identified based on the bone metastatic potential. The effect of cancer was easily identified based on the growth level of the bones. Bone metastases analysis was performed to identify to level of breast cancer. Onken et al. [13] has identified the bone tumor based on the metastatic dissemination pattern analysis. Here, the patterns of different tumor regions were grouped and used for evaluation. The level of instability of the bone cancer patients were identified and used for the classification.

Gong et al. [14] analyzed the patients with bone metastases for the identification of lung cancer. The prognostic factors associated with bone metastases was used for the study. It was identified that the bone metastases associated with the spine was around 64.7%. Zhang et al. [15] presented a methodology for the identification of signaling pathways in the integrated analysis of bone metastases. The potential genes responsible for the occurrence of bone metastases was identified in this research. It was found that the chances of breast cancer were high for the patients having bone metastases. Landi et al. [16] presented a scheme for the immunotherapy for the bone cancer patients. The relationship between bone metastases and lung cancer was identified in this research. Further, the non-small-cell category of lung cancer was evaluated and analyzed.

Palmerini et al. [17] has introduced a framework for the identification of malignancy in the cell tumor of bone. It was identified that giant cell tumor was associated with benign tumor and small cell tumor was greatly

associated with the malignant bone tumor category. Mohaidat et al. [18] presented the challenges involved in the diagnosis of aneurysmal bone cyst. The pathological features of this type of cyst were analyzed. The age and location of occurrence of this type of bone cyst was evaluated by conducting survey with multiple patients.

Larbi et al. [19] utilized the MRI scans for the assessment of involvement of bones in the prostate cancer. The diagnostic accuracies of multiple techniques were compared. The inversion recovery rate was also computed along with the diffusion-weighted sequences. Zheng et al. [20] conducted a study with 13,541 patients for the evaluation of bone metastases. The overall survival rat of bone metastases was calculated in this study. Further, the mortality hazard ratio was evaluated using the data collected from these patients.

### 3. Proposed Methodology

The proposed recurrent neural network-based bone image classification (RNNBIC) methodology comprises of steps like image preprocessing (filtration and enhancement), segmentation, feature extraction and classification.

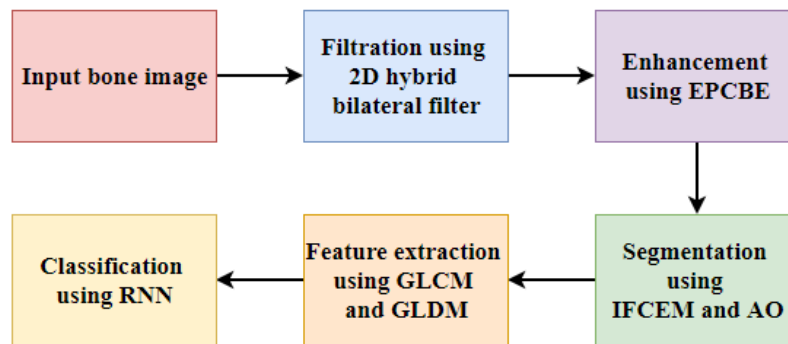


Figure 1. Flow chart of the proposed bone image classification methodology

Figure 1 shows the flow chart of the proposed RNNBIC bone image classification methodology. In this scheme the first step is the acquisition of bone image. The next step is the filtration using 2D Hybrid Bilateral filter. The third step is enhancement using proposed Edge Preservation based Contrast and Brightness Equalization (EPCBE) algorithm. The next step is the clustering using Improved Fuzzy C Expectation Maximization (IFCEM) algorithm and thresholding is done using adaptive Otsu (AO) thresholding algorithm. Then, the Grey level Co-occurrence matrix (GLCM) and Grey level difference method (GLDM) features are extracted. Finally, the classification is done using RNN network architecture.

#### 3.1. Image Pre-processing

Pre-processing was performed using two steps namely, filtration and enhancement. Image filtration was performed using a new 2D Hybrid Bilateral filter and enhancement was performed using the proposed Edge Preservation based Contrast and Brightness Equalization (EPCBE) algorithm.

##### 3.1.1. Image Filtering using 2D Hybrid Bilateral filter

Image filtration was performed using a new 2D Hybrid Bilateral filter. The proposed 2D Hybrid Bilateral filter was designed based on the hybridization of bilateral filter and the adaptive mean adjustment filter. Let us consider the input image to be represented as  $X \in R^{M \times N}$ . The proposed 2D Hybrid Bilateral filter operation is represented as

$$y[m, n] = \left[ \sum_k \sum_l R^{-1}(k, l) T[h_d(m, n; k, l)] * T[h_r(x[m, n], x[k, l])] x[k, l] \right] \quad (1)$$

Where  $h_d$  and  $h_r$  represents domain and range filters respectively. The transform function is represented a

$$T(h_d(m, n)) = e^{-\left(\frac{(m * h)^2 + (n * x_{\max})^2}{2\sigma_d^2}\right)} \quad (2)$$

$$T(h_r(m, n)) = e^{-\left(\frac{(x[m, n] * h - x_{\min} * h)^2}{2\sigma_r^2}\right)} \quad (3)$$

Also,  $\sigma_d$  and  $\sigma_r$  represents the standard deviation of the domain and range filter respectively, the  $x_{\max}$  and  $x_{\min}$  are the minimum and maximum mean values in the 3x3 non-overlapping blocks, and  $h$  is the highest grey scale value in the image. The filtered image is represented as  $Y \in R^{M \times N}$ .

### 3.1.2. Image Enhancement using Edge Preservation based Contrast and Brightness Equalization (EPCBE)

The filtered images were then enhanced using the proposed Edge Preservation based Contrast and Brightness Equalization (EPCBE) algorithm. In this algorithm, histogram of the image was computed and the histogram was equalized such that edges were preserved. Finally, histogram normalization was done to preserve the contrast and the brightness of the image.

#### Algorithm 1: Proposed EPCBE algorithm

**Input:** Filtered image  $Y \in R^{M \times N}$ .

**Output:** Enhanced image  $E \in R^{M \times N}$ .

#### Steps:

- Compute the histogram of the filtered image as

$$h(i) = n\{i\} \quad (4)$$

Where  $n\{i\}$  represents the number of pixels having an intensity of  $i$ .

- Equalize the histogram using

$$h'(i) = \frac{h(i) + \max\{h(i)\}}{h(i) - \min\{h(i)\}} \quad (5)$$

- Normalize the equalized histogram using

$$\bar{h}(i) = \frac{h'(i)}{1/N \sum_{k=0}^i n\{i\}} \quad (6)$$

- Construct the enhanced image  $E \in R^{M \times N}$  using the equalized histogram  $\bar{h}(i)$ .

### 3.2. Segmentation

Segmentation is performed using clustering and thresholding techniques. In this research, image clustering was performed using Improved Fuzzy C Expectation Maximization (IFCEM) algorithm and thresholding was done using adaptive Otsu (AO) thresholding algorithm.

#### 3.2.1. Improved Fuzzy C Expectation Maximization (IFCEM) Algorithm

We have proposed a novel algorithm called Improved Fuzzy C Expectation Maximization (IFCEM). This technique is used for the formation of clusters that can be used for the segmentation and separation of bone cancer regions from the bone images. The proposed IFCEM algorithm is on the traditional Expectation Maximum algorithm [21]. In this algorithm, there are two main steps that are described below.

**Expectation step:**

The probability that a pixel at  $I^E(u, v)$  belongs to a particular Gaussian  $G_i$  with mean  $\mu_i$  and standard deviation  $\sigma_i$  is given by

$$P_{uv}^i = \frac{\exp\left(-\frac{(I^E(u, v) - \mu_i)^2}{2\sigma_i^2}\right)}{\sum_{j=1}^V \exp\left(-\frac{(I^E(u, v) - \mu_j)^2}{2\sigma_j^2}\right)} \tag{7}$$

**Maximization step:**

In this step, the mean  $\mu_i$  and standard deviation  $\sigma_i$  of Gaussian  $G_i$  are estimated again using

$$\mu_i = \frac{1}{Z} \sum_{u,v} P_{uv}^i I^E(u, v) \tag{8}$$

$$\sigma_i = \sqrt{\frac{\sum_{u,v} P_{uv}^i (I^E(u, v) - \mu_i)^2}{Z}} \tag{9}$$

In the proposed algorithm, the initial values for the computation of clusters are computed based on improved Fuzzy C-means clustering algorithm [22], that is given by,

$$J = \sum_{i=0}^H \sum_{n=1}^N \sum_{q=1}^C f_{nq} ED_{nq} MD(i, q) \tag{10}$$

Where  $H$  represents the histogram bin,  $N$  is the number of data points and  $C$  is the number of clusters. The  $f_{nq}$  is the fuzzy membership function between the  $n$ th data point and the  $q$ th cluster,  $ED_{nq}$  is the Euclidean distance between the  $n$ th data point and the  $q$ th cluster and  $MD(i, q)$  is the Manhattan distance between the  $i$ th histogram bin and the  $q$ th cluster.

**3.2.2. Adaptive Otsu (AO) Thresholding**

Otsu threshold is a widely technique for image segmentation. In this technique, a single global threshold is identified for the segmentation of images into the foreground and the background categories. In the proposed adaptive thresholding technique, there is not a single threshold, but an adaptively varying threshold. In this scheme, the image is divided into non-overlapping blocks of size  $5 \times 5$ . For each block the threshold for the segmentation is computed as

$$T_{B_i} = \lambda * \frac{G_{\max} - G_{\min}}{2} \tag{11}$$

Where  $\lambda$  is the variance of the block  $B_i$ ,  $G_{\max}$  is the maximum grey scale value in the block  $B_i$  and  $G_{\min}$  is the minimum grey scale value of the block  $B_i$ .

### 3.3. Feature Extraction

In this work, we have extracted GLCM features [23] and GLDM features [24].

#### 3.3.1. GLCM

GLCM (Grey level Co-occurrence matrix) feature identifies the spatial relationship between the pixels of an image. This feature has a fast-changing range for images having smooth texture and a slow changing range for images with coarse textures. It is computed as

$$GC(m, n) = \frac{\#\{(m_1, n_1), (m_2, n_2)\} \in S \mid f(m_1, n_1) = g_1 \ \& \ f(m_2, n_2) = g_2\}}{\#S} \tag{12}$$

#### 3.3.2. GLDM

GLDM (Grey level difference method) matrix is based on the difference between two pixels that are separated using displacement  $\psi$ . This displacement is computed based on the probability density function and is given by

$$GD = P[I_\psi(x, y) = i] \tag{13}$$

Using these two techniques, two matrices were constructed. From these matrices, several statistical features listed in Table 1 were extracted.

Table 1. Feature extraction using GLCM and GLDM matrix

Feature type	Matrix type	#features
Contrast	GLCM	2
	GLDM	
Correlation	GLCM	2
	GLDM	
Energy	GLCM	2
	GLDM	
Homogeneity	GLCM	2
	GLDM	
Entropy	GLCM	2
	GLDM	
Variance	GLCM	2
	GLDM	
Mean	GLCM	2
	GLDM	
Standard deviation	GLCM	2
	GLDM	
<b>Total # features</b>		<b>16</b>

### 3.4. Classification

The above-mentioned features are computed from the segmented regions. Based on the features extracted from the malignant and benign bone cancer images, Recurrent Neural Network (RNN) structure was constructed as shown in Figure 2. The proposed RNN structure has a hierarchical classification architecture. It is used for the classification of images into two levels, namely benign and malignant. The first level is the benign level and the second is the malignant level. The input bone image is given as input to the convolutional neural network (CNN), that is used for the generation of weights  $w_0$  and  $w_1$  for the long short term memory cells (LSTM). The other input to the first LSTM cell includes the input parameters  $u_0$  and  $v_0$ . The classified benign output of the first hierarchical unit is given as input to the second unit. This unit is used for the identification of malignant cases.

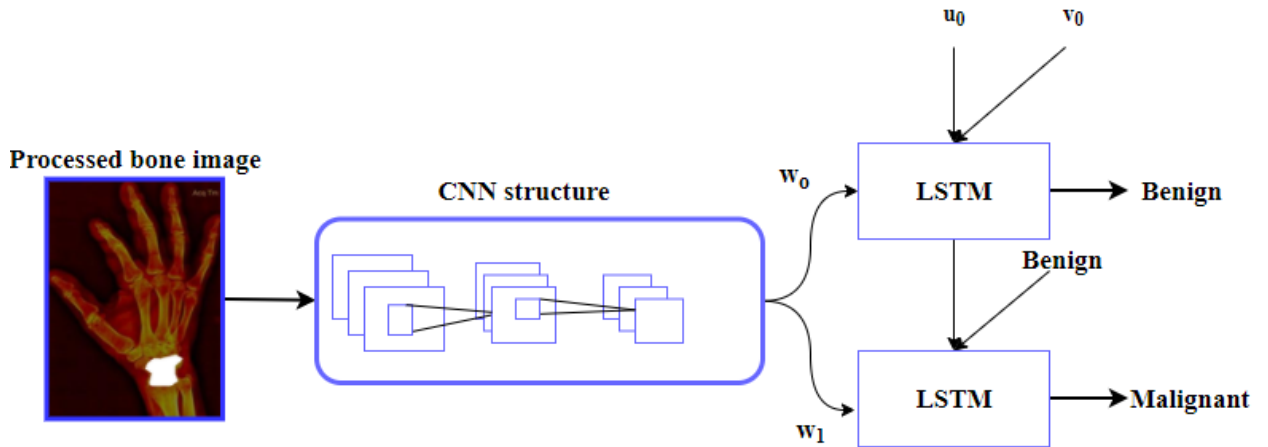


Figure 2. Architecture of the proposed RNN structure

#### 4. Results and Discussion

##### 4.1. Parameter Settings

The proposed system was simulated using MATLAB software running on windows intel i3 core processor with 4GB RAM.

##### 4.2. Simulation Results

Figure 3 shows the sample input noisy bone images. These images contain noise components and require proper processing before feature extraction.



Figure 3. Input images

Figure 4 shows the image filtered using the 2D Hybrid bilateral filter. The filtration operation helps in the removal of noise from the image.



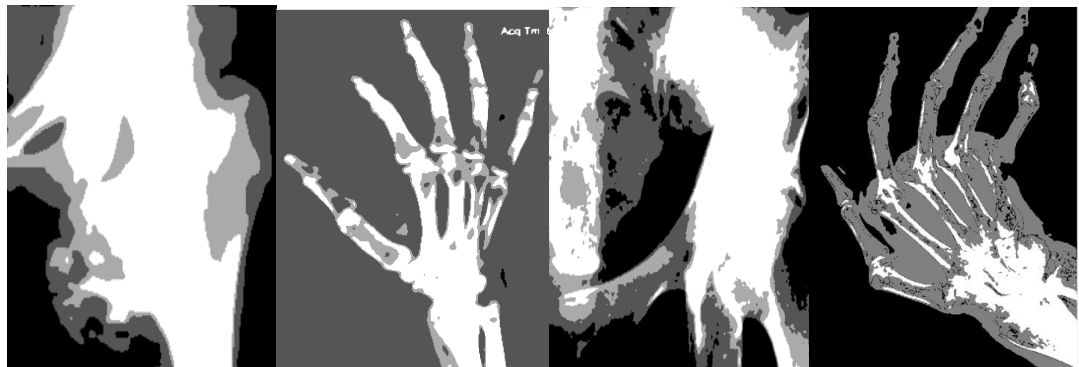
**Figure 4. Images filtered using 2D Hybrid Bilateral filter**

Figure 5 shows the image enhanced using the EPCBE algorithm. The enhancement operation helps in the creation of images with better contrast.



**Figure 5. Images enhanced using EPCBE algorithm**

Figure 6 shows the clustered images using the IFCEM algorithm. The formation of clusters helps in the identification of bone cancer regions.



**Figure 6. Images clustered using IFCEM algorithm**

Figure 7 shows the segmentation results obtained using adaptive Otsu thresholding algorithm. These regions clearly show the specific areas of bone cancer.



**Figure 7. Segmentation results using AO thresholding**

Figure 8 shows the images that are formed using the superimposition of the input and the output segmented results. These images acts as discriminative inputs for the extracted of features.



**Figure 8. Superimposition of input and output segmented results**

### 4.3. Quantitative Analysis

#### 4.3.1 Evaluation of Proposed Filtration Technique

The proposed image filtration using 2D Hybrid Bilateral Filter is evaluated using metrics like MSE and PSNR. From Table 2 we observe that, the 2D median filter achieves an average MSE of 7.71, 2D adaptive median filter attains MSE of 3.48 and the proposed scheme achieves a mean MSE of 0.87.

**Table 2. Performance evaluation using Mean Square Error**

Images	MSE		
	2D Median Filter	2D Adaptive Median Filter	Proposed 2D Hybrid Bilateral Filter
<b>Image 1</b>	8.12	3.08	0.85
<b>Image 2</b>	7.89	3.31	0.84
<b>Image 3</b>	7.21	3.42	0.88
<b>Image 4</b>	7.62	4.12	0.91

Table 3 shows the performance evaluation using peak signal to noise ratio. From Table 3 we observe that, the 2D median filter achieves an average PSNR of 22.32, 2D adaptive median filter attains PSNR of 21.12 and the proposed scheme achieves a mean PSNR of 31.82.

**Table 3. Performance evaluation using PSNR**

Images	PSNR (in dB)		
	2D Median Filter	2D Adaptive Median Filter	Proposed 2D Hybrid Bilateral filter
<b>Image 1</b>	21.02	23.42	34.21
<b>Image 2</b>	22.22	21.53	31.53
<b>Image 3</b>	23.51	20.21	30.32
<b>Image 4</b>	22.55	19.32	31.22

**4.3.2. Evaluation of Segmentation Algorithms**

Evaluation of the proposed segmentation algorithm is performed using metrics like Jaccard coefficient and Dice coefficient. Table 4 shows the performance evaluation using Jaccard Coefficient. From Table 4 we infer that, the average value of Jaccard Coefficient for K means clustering with Otsu thresholding was 0.459. Similarly, the average value of Jaccard Coefficient for Fuzzy C Means Clustering with Otsu thresholding was 0.660. But the proposed IFCEM and AO thresholding achieved a maximum Jaccard Coefficient of 0.761. Thus, our proposed framework achieves best performance in terms of Jaccard Coefficient.

**Table 4. Performance evaluation using Jaccard Coefficient**

Images	Jaccard Coefficient		
	K means clustering + Otsu Thresholding	Fuzzy C Means Clustering + Otsu Thresholding	Proposed IFCEM+AO Thresholding
<b>Image 1</b>	0.452	0.693	0.729
<b>Image 2</b>	0.462	0.624	0.803
<b>Image 3</b>	0.479	0.641	0.731
<b>Image 4</b>	0.446	0.683	0.783

Table 5 shows the performance evaluation using Dice Coefficient. From Table 5 we infer that, the average value of Dice Coefficient for K means clustering with Otsu thresholding was 0.543. Similarly, the average value of Dice Coefficient for Fuzzy C Means Clustering with Otsu thresholding was 0.686. But the proposed IFCEM and AO thresholding achieved a maximum Dice Coefficient of 0.823. Thus, our proposed framework achieves best performance in terms of Dice Coefficient.

**Table 5. Performance evaluation using Dice Coefficient**

Images	Dice Coefficient		
	K means clustering + Otsu Thresholding	Fuzzy C Means Clustering + Otsu Thresholding	Proposed IFCEM+AO Thresholding
Image 1	0.593	0.632	0.832
Image 2	0.595	0.765	0.732
Image 3	0.491	0.662	0.856
Image 4	0.495	0.687	0.875

**4.3.3. Evaluation of Classification Algorithms**

For performance evaluation of the classification algorithm, metrics like overall accuracy, recall, precision, specificity and F-score were calculated. Table 6 shows the results obtained in terms of overall accuracy. From Table 6, we see that RNN algorithm produces the best results compared to all other traditional classification algorithms with highest accuracy of 96.59%.

**Table 6. Comparison of classification Accuracy**

Classification algorithms	Classification Accuracy (%)
k-NN	85.72
SVM	88.63
LR	91.61
SRC	93.79
RNN	<b>96.59</b>

Figure 9 represents the comparison of specificity using the proposed classification algorithm. It is clear that standard algorithms like k-nearest neighbor (k-NN), support vector machine (SVM), logistic regression (LR) and sparse representation-based classification (SRC) achieves specificity rate of 78.93%, 82.56%, 91.32% and 93.92% respectively. However, the proposed RNN classifier attains a high specificity of 96.25%.



**Figure 9. Comparison of specificity**

Figure 10 represents the comparison of precision using the proposed classification algorithm. It is clear that standard algorithms like k-nearest neighbor (k-NN), support vector machine (SVM), logistic regression (LR) and sparse representation-based classification (SRC) achieves precision rate of 77.83%, 89.23%, 91.47% and 94.90% respectively. However, the proposed RNN classifier attains a high precision of 95.83%.



**Figure 10. Comparison of precision**

Figure 11 represents the comparison of recall using the proposed classification algorithm. It is clear that standard algorithms like k-nearest neighbor (k-NN), support vector machine (SVM), logistic regression (LR) and sparse representation-based classification (SRC) achieves recall rate of 81.32%, 88.64%, 91.74% and 93.72% respectively. However, the proposed RNN classifier attains a high recall of 96.52%.



**Figure 11. Comparison of recall**

Figure 12 represents the comparison of F-score using the proposed classification algorithm. It is clear that standard algorithms like k-nearest neighbor (k-NN), support vector machine (SVM), logistic regression (LR) and sparse representation-based classification (SRC) achieves F-score rate of 91.32%, 92.43%, 94.93% and 94.99% respectively. However, the proposed RNN classifier attains a high F-score of 96.34%.



**Figure 12. Comparison of F-score**

Table 7 represents the comparison of classification time using the proposed classification algorithm. It is clear that standard algorithms like k-nearest neighbor (k-NN), support vector machine (SVM), logistic regression (LR) and sparse representation-based classification (SRC) achieves high classification time of 24.1ms, 19.5ms, 18.4ms and 15.5ms respectively. However, the proposed RNN classifier attains least classification time of 9.7ms.

**Table 7. Comparison of classification time**

Classification algorithms	Classification time (ms)
k-NN	24.1
SVM	19.5
LR	18.4
SRC	15.5
RNN	9.7

## 5. Conclusion

In this research we have proposed a new methodology for the classification of bone cancer images. Here, 2D Hybrid Bilateral filter was used for image filtration. The filtered images were enhanced using proposed Edge Preservation based Contrast and Brightness Equalization (EPCBE) algorithm. The enhanced images were segmented based on Improved Fuzzy C Expectation Maximization (IFCEM) algorithm and adaptive Otsu (AO) thresholding algorithm. The input images were superimposed with the segmentation results to form the processed bone images. The processed images were used for the extraction of Grey level Co-occurrence matrix (GLCM) and Grey level difference method (GLDM) matrices. From these matrices, various statistical features were extracted. Finally, the classification was done using RNN network architecture. Performance evaluation revealed that the proposed methodology produces accurate bone cancer diagnosis results. The images were classified into benign and malignant categories. The proposed scheme achieved values of about 0.87, 31.82, 0.761 and 0.823 in terms of MSE, PSNR, Jaccard coefficient and Dice coefficient respectively. Further, the proposed RNN classifier attained high rates of 96.59%, 96.25%, 95.83%, 96.52% and 96.34% in terms of accuracy, specificity, precision, recall and F-score respectively.

## Reference

- [1] G. T. da Silva, A. Bergmann, and L. C. S. Thuler, "Incidence and risk factors for bone metastasis in Non-Small Cell Lung Cancer," *Asian Pacific J. Cancer Prev.*, vol. 20, no. 1, pp. 45–51, 2019, doi: 10.31557/APJCP.2019.20.1.45.
- [2] P. P. Acharya, D. Sarma, and B. McKinnon, "Trends of temporal bone cancer: SEER database," *Am. J. Otolaryngol. - Head Neck Med. Surg.*, vol. 41, no. 1, p. 102297, 2020, doi: 10.1016/j.amjoto.2019.102297.
- [3] V. M. Wu, E. Huynh, S. Tang, and V. Uskoković, "Brain and bone cancer targeting by a ferrofluid composed of superparamagnetic iron-oxide/silica/carbon nanoparticles (earthicles)," *Acta Biomater.*, vol. 88, pp. 422–447, 2019, doi: 10.1016/j.actbio.2019.01.064.
- [4] A. Martins *et al.*, "Qualitative study exploring patients experiences of being diagnosed and living with primary bone cancer in the UK," *BMJ Open*, vol. 9, no. 9, pp. 1–10, 2019, doi: 10.1136/bmjopen-2018-028693.
- [5] L. M. S. Boevé *et al.*, "Effect on Survival of Androgen Deprivation Therapy Alone Compared to Androgen Deprivation Therapy Combined with Concurrent Radiation Therapy to the Prostate in Patients with Primary Bone Metastatic Prostate Cancer in a Prospective Randomised Clinical Trial: Data from the HORRAD Trial," *Eur. Urol.*, vol. 75, no. 3, pp. 410–418, 2019, doi: 10.1016/j.eururo.2018.09.008.
- [6] N. Otsu, "Threshold Selection Method From Gray-Level Histograms.," *IEEE Trans Syst Man Cybern*, vol. SMC-9, no. 1, pp. 62–66, 1979, doi: 10.1109/tsmc.1979.4310076.

## Bone Mineral Density Measurement for Detection of Bone Cancer Using Recurrent

- [7] O. Nicolatou-Galitis *et al.*, “Medication-related osteonecrosis of the jaw: definition and best practice for prevention, diagnosis, and treatment,” *Oral Surg. Oral Med. Oral Pathol. Oral Radiol.*, vol. 127, no. 2, pp. 117–135, 2019, doi: 10.1016/j.oooo.2018.09.008.
- [8] J. Zhou, Z. Gou, R. Wu, Y. Yuan, G. Yu, and Y. Zhao, “Comparison of PSMA-PET/CT, choline-PET/CT, NaF-PET/CT, MRI, and bone scintigraphy in the diagnosis of bone metastases in patients with prostate cancer: a systematic review and meta-analysis,” *Skeletal Radiol.*, vol. 48, no. 12, pp. 1915–1924, 2019, doi: 10.1007/s00256-019-03230-z.
- [9] F. Ruatta *et al.*, “Prognosis of renal cell carcinoma with bone metastases: Experience from a large cancer centre,” *Eur. J. Cancer*, vol. 107, pp. 79–85, 2019, doi: 10.1016/j.ejca.2018.10.023.
- [10] M. Moradi, M. Abdolhosseini, A. Zarrabi, and B. Johari, “A review on application of Nano-structures and Nano-objects with high potential for managing different aspects of bone malignancies,” *Nano-Structures and Nano-Objects*, vol. 19, no. 27, p. 100348, 2019, doi: 10.1016/j.nanoso.2019.100348.
- [11] O. Bandyopadhyay, A. Biswas, and B. B. Bhattacharya, “Bone-Cancer Assessment and Destruction Pattern Analysis in Long-Bone X-ray Image,” *J. Digit. Imaging*, vol. 32, no. 2, pp. 300–313, 2019, doi: 10.1007/s10278-018-0145-0.
- [12] N. Urbano, M. Scimeca, E. Bonanno, and O. Schillaci, “<sup>99m</sup>Tc sestamibi SPECT: A possible tool for early detection of breast cancer lesions with high bone metastatic potential,” *Futur. Oncol.*, vol. 15, no. 5, pp. 455–457, 2019, doi: 10.2217/fon-2018-0735.
- [13] J. S. Onken, L. S. Fekonja, R. Wehowsky, V. Hubertus, and P. Vajkoczy, “Metastatic dissemination patterns of different primary tumors to the spine and other bones,” *Clin. Exp. Metastasis*, vol. 36, no. 6, pp. 493–498, 2019, doi: 10.1007/s10585-019-09987-w.
- [14] L. Gong, L. Xu, Z. Yuan, Z. Wang, L. Zhao, and P. Wang, “Clinical outcome for small cell lung cancer patients with bone metastases at the time of diagnosis,” *J. Bone Oncol.*, vol. 19, no. November, p. 100265, 2019, doi: 10.1016/j.jbo.2019.100265.
- [15] Y. Zhang, W. He, and S. Zhang, “Seeking for correlative genes and signaling pathways with bone metastasis from breast cancer by integrated analysis,” *Front. Oncol.*, vol. 9, no. MAR, pp. 1–13, 2019, doi: 10.3389/fonc.2019.00138.
- [16] L. Landi *et al.*, “Bone metastases and immunotherapy in patients with advanced non-small-cell lung cancer,” *J. Immunother. Cancer*, vol. 7, no. 1, pp. 1–9, 2019, doi: 10.1186/s40425-019-0793-8.
- [17] E. Palmerini, P. Picci, P. Reichardt, and G. Downey, “Malignancy in Giant Cell Tumor of Bone: A Review of the Literature,” *Technol. Cancer Res. Treat.*, vol. 18, pp. 1–9, 2019, doi: 10.1177/1533033819840000.
- [18] Z. M. Mohaidat, S. R. Al-Gharaibeh, O. N. Aljararhih, M. T. Nusairat, and A. A. Al-Omari, “Challenges in the Diagnosis and Treatment of Aneurysmal Bone Cyst in Patients with Unusual Features,” *Adv. Orthop.*, vol. 2019, 2019, doi: 10.1155/2019/2905671.
- [19] A. Larbi *et al.*, “Whole-body MRI to assess bone involvement in prostate cancer and multiple myeloma: comparison of the diagnostic accuracies of the T1, short tau inversion recovery (STIR), and high b-values diffusion-weighted imaging (DWI) sequences,” *Eur. Radiol.*, vol. 29, no. 8, pp. 4503–4513, 2019, doi: 10.1007/s00330-018-5796-1.
- [20] X. Q. Zheng *et al.*, “Incidence, prognostic factors, and a nomogram of lung cancer with bone metastasis at initial diagnosis: A population-based study,” *Transl. Lung Cancer Res.*, vol. 8, no. 4, pp. 367–379, 2019, doi: 10.21037/tlcr.2019.08.16.
- [21] A. P. Dempster, N. M. Laird, and D. B. Rubin, “Maximum Likelihood from Incomplete Data Via the EM Algorithm,” *J. R. Stat. Soc. Ser. B*, vol. 39, no. 1, pp. 1–22, 1977, doi: 10.1111/j.2517-6161.1977.tb01600.x.

- [22] Y. Zheng, B. Jeon, D. Xu, Q. M. J. Wu, and H. Zhang, "Image segmentation by generalized hierarchical fuzzy C-means algorithm," *J. Intell. Fuzzy Syst.*, vol. 28, no. 2, pp. 961–973, 2015, doi: 10.3233/IFS-141378.
- [23] X. Zhang, J. Cui, W. Wang, and C. Lin, "A study for texture feature extraction of high-resolution satellite images based on a direction measure and gray level co-occurrence matrix fusion algorithm," *Sensors (Switzerland)*, vol. 17, no. 7, 2017, doi: 10.3390/s17071474.
- [24] J. S. Weszka, C. R. Dyer, and A. Rosenfeld, "A Comparative Study of Texture Measures for Terrain Classification," *IEEE Trans. Syst. Man Cybern.*, vol. SMC-6, no. 4, pp. 269–285, 1976, doi: 10.1109/TSMC.1976.5408777.